Observation of Parity Violation in Cosmic Anti-muon Weak Decay

Y. Watanabe, J. Ho, W. Duan, M. Nero
Elementary Particle Physics Lab, University of California Los Angeles

March 19, 2018

Abstract

This experiment verifies violation of parity in cosmic anti-muon weak decay. Parity violation is detected by measuring a non-zero mean product of an axial vector $\hat{\sigma}$, which is the spin vector of anti-muon, and a polar vector $\hat{p}$, which is the unit momentum vector of the produced positron. Specifically, this experiment observes $\hat{p}$ to oscillate at Larmor frequency in phase with the precession of $\hat{\sigma}$ in a uniform magnetic field. Evidence for parity violation is observed with a p-value of 0.572 ± 0.169. Although not executed, this result could potentially be applied to measure the anti-muon magnetic moment.

1 Introduction and Theory

Parity invariance is a discrete symmetry possessed by all fundamental interactions except the weak interaction. Parity invariance of a physical process requires the mirror image of the process to also represent a perfectly possible physical process [Gri08]. In practice, however, all weak interactions violate parity invariance. This experiment observes the parity violation in cosmic anti-muon weak decay. The decay is described by

$$\mu^+ \to e^+ + \nu_e + \bar{\nu}_\mu, \tag{1}$$

As parity transformation reverses the sign of polar vectors like $\vec{r}$ and $\vec{p}$ and maintains the sign of axial vectors like $\vec{L}$ and $\vec{s}$, parity invariance requires the scalar product of an axial vector and a polar vector to be zero. More generally, the mean of the product is required to be zero, if either observable has a non-singular probability distribution. Parity violation is thus shown when the axial momentum unit vector $\hat{p}$ of the produced positron has a non-zero mean $\langle \hat{p} \rangle$ aligned with the polar anti-muon spin unit vector $\hat{\sigma}$. Thus, a non-zero positive value of $\langle \hat{\sigma} \cdot \hat{p} \rangle$ indicates a parity violation in the anti-muon decay.

The anti-muon source for the experiment needs to be polarized in spin direction, because an isotropic distribution of individual spin would completely shield any possible asymmetry in the angular distribution of the produced positron with respect to the spin direction. This experiment thus uses cosmic muon rays, in which anti-muons are polarized upwards in the lab frame by roughly 20%[OS17]. Figure 1 presents the measured polarization of cosmic muon spin of previous studies.

In this experiment, polarized cosmic anti-muons of roughly 230 MeV momentum are stopped in a copper target, at which a horizontal uniform magnetic field B is applied. According to quantum mechanics, the expectation of the muon spin vector $\langle \mathbf{S} \rangle$ will precess about the magnetic field line at the Larmor frequency ω, which is given by

$$\omega = \gamma B, \tag{2}$$

where γ represents the gyromagnetic ratio. As the mean spin direction precesses around the magnetic field line, the decay time t, or the time between the detection of a stopped muon and the detection of a decay, is recorded. Depending on the resultant positron momentum, these decay events are categorized into up and down events accordingly. By observing the oscillation in the numbers of up and down events with respect to decay time t, this experiment establishes the asymmetric correlation between $\langle \mathbf{S} \rangle$ and $\hat{p}_z$, and thereby observes the violation of parity in anti-muon weak decay. Finally, from the measured Larmor frequency ω and the applied field B, the magnetic moment $\boldsymbol{\mu}$ of the anti-muon can be experimentally determined by the relation

$$\boldsymbol{\mu} = \gamma \mathbf{S}. \tag{3}$$

The charged cosmic rays detected on earth's surface comprises primarily muons and anti-muons. Because the detectors used do not distinguish a positive charged particle from a negative one, the decay of

cosmic muons μ^- may neutralize the measurement of a non-zero $\langle \hat{\sigma} \cdot \hat{p} \rangle$ of the anti-muon. This undesirable μ^- background is largely reduced by choosing copper as the target material to stop cosmic particles of selected energy. Besides weak decay, μ^- additionally interacts with the copper nucleus by

$$\mu^- + p \to \nu_\mu + n. \tag{4}$$

This reaction in copper has a characteristic time of around 160 ns, which is less than one-tenth of the mean lifetime of the anti-muon weak decay (2200 ns) [OS17]. Thus, most of the stopped muons μ^- are quickly absorbed in the target, which allows us to better observe the μ^+ decay for later times.

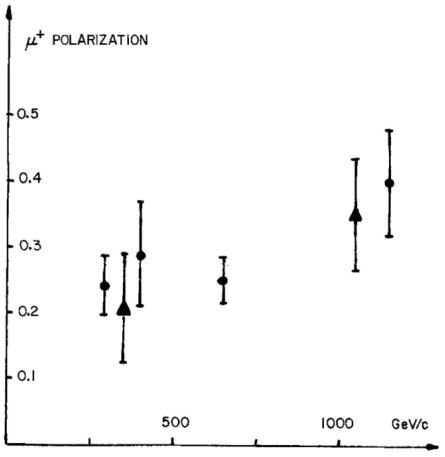

Figure 1: **Measured Muon Polarization on Sea Level by Previous Studies.** The triangles represent measurement made by Alikhanyan [Ali59], and circles by Dolgoshein *et al.* [DLU62]

2 Experimental Arrangement and Procedure

2.1 Experiment Setup

This experiment uses five plastic scintillation counters and photomultiplier tubes (PMT) which are attached to the end of the counters to detect any charged particles going through specific regions. In summary, charged particles going through a counter produces scintillation light that is detected by the PMT, which outputs an analog signal. This signal is converted into a digital one when it passes through a discriminator, which produces a standard NIM level pulse of a specified width of 20 ns. The five counters and PMTs are arranged as in Figure 2.

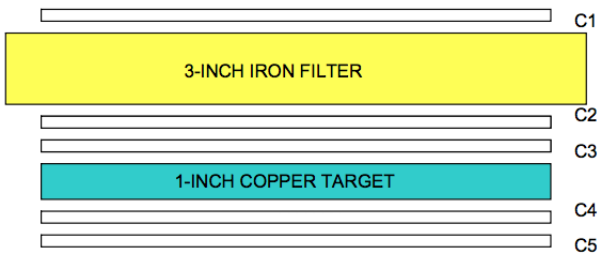

Figure 2: **Experimental Setup** [OS17] In the figure, cosmic muons travel downward. C1 to C5 represent five slab scintillators. The iron filter has a larger area, and the copper target has a smaller area than each scintillator to reduce the chance of a muon landing on the target while evading the scintillators.

As shown in Figure 2, a 7.6 ± 0.5 cm thick iron plate is positioned between detector 1 and 2 to keep cosmic muons with momentum less than 200 ± 10 MeV from reaching the target. The 2.5 ± 0.5 cm thick copper target stops muons with initial momentum less than 230 ± 10 MeV inside the target.

There are three primary events in this experiment. Event M indicates that a anti-muon stopped in the copper target. U indicates that the positron produced from Equation 1 was up-going, and D indicates that it was down-going. We ascertain these events by the coincidence of detection signals from a specific combination of detectors. The details are listed in Table 1 below.

Event Name	Condition of Detectors
Stopped μ^+ (M)	1, 2, 3, $\bar{4}$
Up-going e^+ (U)	$\bar{1}$, 2, 3, $\bar{4}$
Down-going e^+ (D)	$\bar{1}$, $\bar{3}$, 4, 5

Table 1: **Conditions for Registering Events** Numbers indicate a normal signal from its corresponding counter, while a number with a bar above it indicates the complementary signal from its corresponding detector. E.g. an event M requires detectors 1, 2, 3 to be triggered and detector 4 to not be triggered simultaneously.

Note that U and D events require a null signal from detector 1 to exclude contaminated events, which occur when a second muon penetrates detector 1 after a registered M event.

In this experiment, a registered M event starts two time-to-digital converters (TDC) for events U and D respectively. It also opens a 20 μs gate for U and D

events, which corresponds to 10 lifetimes of an anti-muon. The triggering of a U or D event will then stop the corresponding TDC timer. After these 20 μs, the label and the measured time interval of the TDC that stops first are recorded by a computer, and the experiment device returns to detect M events for the next measurement. In the case where neither of the TDCs are stopped within 20 μs, no measurement is recorded. The precision of the TDC used is 20 ns, and the width of a typical digital signal in the circuit is 20 ns as well. The veto signals has widths of 50 ns, and the coincidence requires signals to overlap at least 5 ns in time.

2.2 Experiment Procedure

The first step of the experiment is to calibrate the PMTs and discriminators for sufficient detection efficiency. As recommended in the setup instructions, the threshold for discriminators that convert analog signals from PMT to digital signals is chosen to be 20 mV [OS17]. However, the high voltage (HV) of each PMT which controls the detector's sensitivity to scintillation light needs to be calibrated to provide enough detection efficiency for charged particles without introducing too many false signals from thermal noise.

To calibrate the PMTs, the singles rate method is first used. For a discriminator threshold of 20mV, the trigger rate for each PMT is plotted as a function of its HV. The results for PMT 1 are displayed below, and the other PMT plots may be seen in the Appendix.

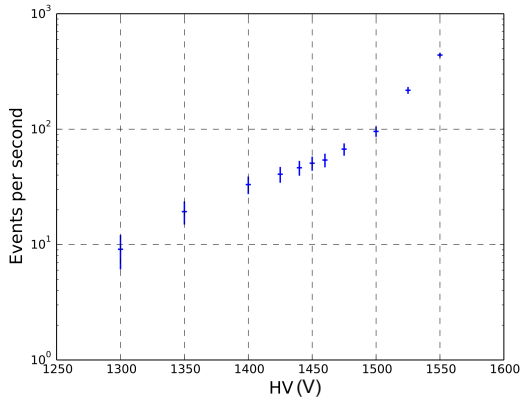

Figure 3: **Single Rates of PMT 1** The logarithm plot shows the dependence of triggering rate of the first PMT on its applied HV. The middle region where the slope is smaller is the PMT's plateau.

As seen in Figure 3 above, at lower voltages, the PMT sensitivity is too small for charged particle signals to be efficiently detected and muon events are missed. As the HV is raised, the PMT gain increases and a plateau region of operation is reached where the PMT is fully efficient at detecting muon events. At higher HVs, noise is introduced, which results in a region of rapidly increasing trigger rate. We found preliminary HVs for every PMT, and then proceeded to the modified coincidence method to ascertain the best HV values for the PMTs. Dual discriminator method was found to give unreliable results, predicting abnormally high HV for the PMTs.

The modified coincidence method utilizes the ratio R given by Equation 5 below.

$$R = \frac{C1 \bigotimes C2 \bigotimes C3}{C1 \bigotimes C3} \tag{5}$$

A good value of HV1 was used, and HV2 and HV3 were set to inefficient values (using our estimated efficient values from the single rates method). HV2 was raised until ratio R plateaus, at which C2 is efficient and only C3 is limiting. HV3 was then raised. If the ratio did not change, it meant that C1, 2 and 3 were efficient. If the ratio decreased, it meant that C3 was becoming more efficient, and thus HV2 was raised again until R plateaued. The same process is repeated using counters 3, 4, and 5.

With estimates from the single rates method, and using the modified coincidence method, initial efficient HV values were obtained. As the PMTs have quite a large plateau before noise is introduced, 50 V were added to these values to ensure efficiency. The final HV values are included in Table 3 in the Appendix. A coincidence method plot for counters 1, 2, and 3 is shown in Figure 4 below, and for counters 3, 4, and 5 may be found in the Appendix.

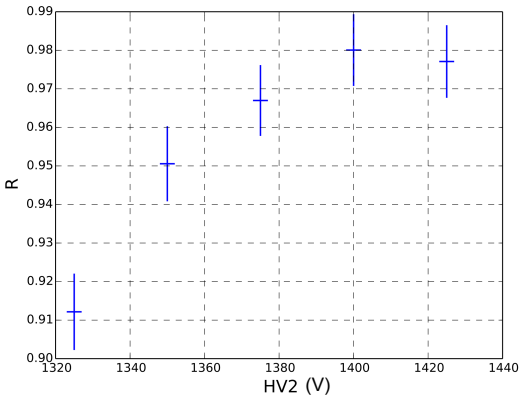

Figure 4: **Measuring Rate by Coincidence Method** The dependence of coincidence rate of C1, 2, and 3 on HV2. PMT 1 and 3 have saturating HVs. Graphs show that for HV2 $>$ 1400 V, it is no longer the limiting factor of the coincidence rate, meaning PMT 2 is efficient.

After plateauing the PMTs, the logic circuit is connected. Analog signals from the five PMTs are converted to digital signals using a set of discriminators with 20 mV threshold and 50 ns output width. Through another set of discriminators with much higher threshold and 20 ns output width, these signals are sharpened, and their coincidence as well as the null signals from the first set discriminators form the M, U, and D events as described in Table 1.

Measurements of the decay time and the produced positron's momentum direction are carried out under three different conditions. The main part of the experiment has the target installed with a controlled current of 3.84 A going through the coils around the target to supply a uniform horizontal magnetic field. In this case, the mean spin vector of the stopped antimuon precesses around the magnetic field before it decays, and the experiment detects the number of up and down events respectively to oscillate in magnitude with respect to the decay time.

Measurements under the other two conditions are carried out to estimate the number of false events and background. The first one has the target installed, but no current going through the coils and therefore no applied magnetic field. The second one has the copper target as well as the coils taken out of the device. The usage of these measurements to do background corrections is described in the following section.

3 Data, Analysis, and Results

The decay time and momentum direction for the produced positron are collected under three different conditions. These conditions, together with the number of events recorded and the total length of data collection time for that particular condition are shown in Table 2 below. The bin size of 200 ns is selected so the magnetic moment precession can be observed, and yet it is not too narrow such that statistical fluctuations are large.

Condition	Number of hours	Total U events	Total D events
Magnet On	370	8,697	6,214
Magnet Off	268	10,655	6,721
Target Out	172	1,735	623

Table 2: **Experiment Measurement Summary** Magnet On gives decay direction precession. Magnet Off and Target Out are used for background subtraction. Magnet Off has a higher event rate compared to Magnet On, as precessing muons are more likely to produce a positron traveling horizontally (which we do not detect).

3.1 Rate Estimation of Stopped Muon

The rate of the M (stopped muon) event is estimated by taking the product of the total cosmic muon flux and the geometric acceptance of the experimental setup.

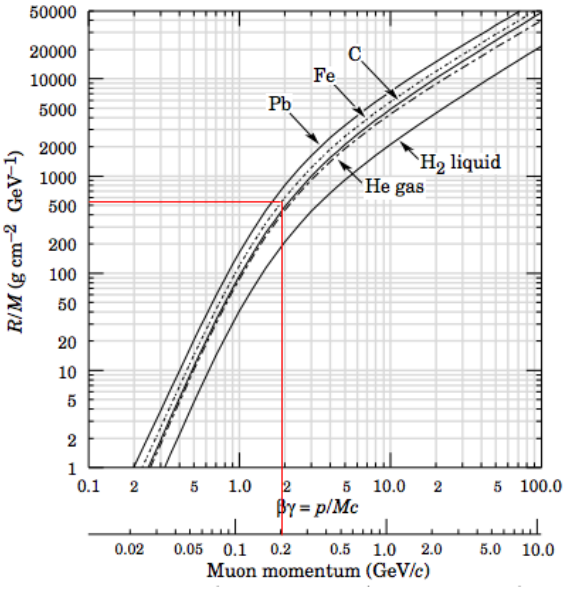

(a) R/M versus Muon Momentum.

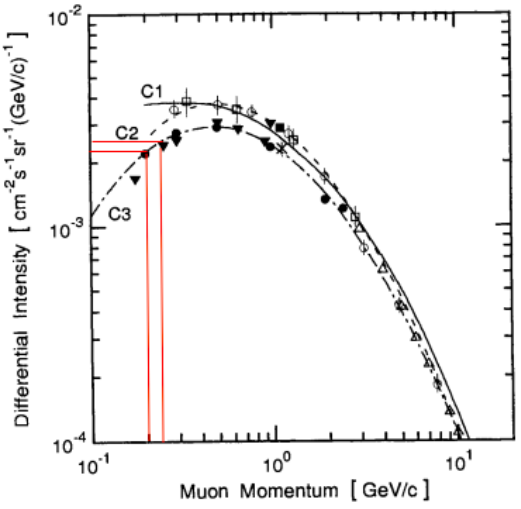

(b) Differential Intensity versus Muon Momentum

Figure 5: **Charts used for calculating rate estimation of stopped muons.[P+17]** These charts are the tools used to calculate the total cosmic muon flux at sea level for our setup. Given the stopping power of the iron filter, (a) allows us to determine the minimum muon momentum to get through the filter. Given the momentum range, integrating the differential intensity curve in (b) allows us to determine the amount of muons reaching sea level within the specified momentum range.

The total flux of cosmic muons is calculated by integrating the sea level differential flux over the momentum range that the hardware selects. For a muon to trigger an M event, it needs enough initial momentum to reach C3, but not enough to get through the copper target and reach C4. The minimum momentum can then be estimated from the stopping power of the iron target (7.6 ± 0.5 cm thick), plus that of scintillators 1 and 2 (2 ± 0.5 cm thick each). The maximum momentum muons penetrate scintillator 3 and the copper target (2.5 ± 0.5 cm thick) without reaching scintillator 4. The online Particle Data Group (PDG) [P+17] booklet provides the measured stopping power per gram of material per unit area for different materials, which indicates that scintillators do not contribute much in this experiment. Referring to Figure 5a, the minimum and maximum muon momenta required to register an M event are estimated to be 200 ± 10 MeV, and 230 ± 10 MeV. The flux per unit solid angle per unit area is then estimated from Figure 5b with the muon momentum range. As the range is quite small, a constant differential intensity of 2.3×10^{-3} cm^{-2}·s^{-1}·sr^{-1}·GeV^{-1} is used. This gives an average flux of

$$\Phi = (6 \pm 2) \times 10^{-5} \text{Hz}/(\text{cm}^{-2} \cdot \text{sr}). \tag{6}$$

For a muon to register a M event, it needs to pass through PMT 1 and land on the copper target, both of which have sizes $l = 55 \pm 5$ by $w = 35 \pm 5$ cm. The separation between the two is 30 ± 3 cm. The relatively large uncertainty in length measurements results from the fact that the scintillators are wrapped in foil to make them light-tight. Applying the simple Monte Carlo simulation [Sul71], the solid angle is estimated to be $\Omega = 1.3 \pm 0.2$ sr, corresponding to an acceptance ($\Omega\times$ Target Area) of 2300 ± 300 sr·cm^2.

Multiplying the average flux in Equation 6 with the acceptance, the expected stopped muon event rate f is calculated to be

$$f = \frac{1}{2} \cdot \Omega \times A \times \Phi = (240 \pm 80)\text{hour}^{-1} \tag{7}$$

in which the fraction $\frac{1}{2}$ comes from the fact that about half of the stopped muons are μ^-, of which approximately 80% are absorbed according to Equation 4. The uncertainty primarily originates from the values inferred from Figure 5a. In comparison, the measured U/D event rate is

$$f' = (47 \pm 5)\text{hour}^{-1}. \tag{8}$$

The discrepancy between f and f' is believed to be due to detector efficiencies. As registration of all events requires coincidence of two detectors (to reduce noise in the recorded measurements), one of the two detectors failing to trigger will cause an event to not be recorded. Since both M and either U or D need to be triggered for a recorded event, all four detectors must trigger effectively for an event to be recorded. For reference, if each detector has an independent detection efficiency of 0.9, then only 65% of the real events will be recorded.

Some other factors that contribute to a theoretical overestimation include muons that decay before the TDC starts (70 ns after muon actually lands), coincident noise triggers in the veto detector, a fast muon landing on C1 after an M event is registered, and long lived muons that decay after the 20 micro second gate assigned by the experiment. However, all these factors are estimated to only be a small correction to the measured rate.

3.2 Background Estimation

There are three major sources of background detections that had to be corrected for. The first is associated with muon μ^- weak decay (conjugation of Equation 1), which are mixed into the μ^+ measurements as the detectors do not distinguish positive particles from negative ones. Due to the short mean lifetime of the μ^- described in Equation 4 of about 160 ns [OS17], stopped μ^- in the copper target decreases in number at a much faster rate than μ^+. Thus, this background is reduced by discarding all decay events before 200 ns in which a relatively large proportion ($\approx 30\%$) of the measurements are in fact μ^- decay.

The second major source of background detections are off target events, which occur when a registered stopped muon stops in detector 3 or the aluminum shelf that supports the detectors, instead of the target. Being outside the target and thus the magnetic field, the anti-muon's spin does not precess around the horizontal axis. To reduce this background, the data collected without the presence of the copper target (or the 'target out' condition, from Table 2), is scaled to match the total data collection time for the magnet on condition, and then subtracted from it for up and down events separately. In addition, this background is dependent on decay time, since the registrations of M and U/D events come from the arrival and decay of the same muon. Thus, the subtraction is be done bin by bin. The scaled target out data centered to the midpoint of each bin is shown in Figure 6 below.

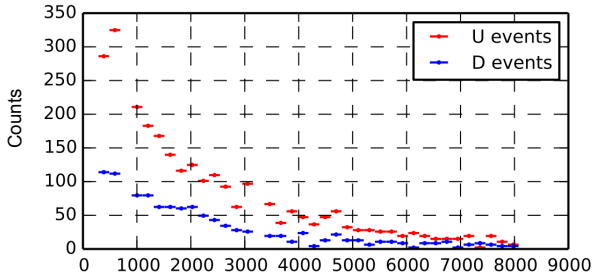

Figure 6: **Scaled target out events per bin (ns)**Measured events are sorted into 200 ns wide bins according to decay time. Uncertainty in a number of events is estimated to be its square root. Uncertainty in time is estimated as half of bin size width. Note that the TDC used for U events gives a very narrow peak centered at 670 ns (less than 60 ns in full width at half maximum). Therefore that bin is excluded from data analysis.

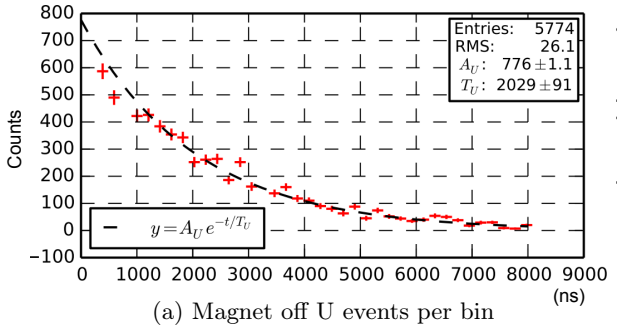

(a) Magnet off U events per bin

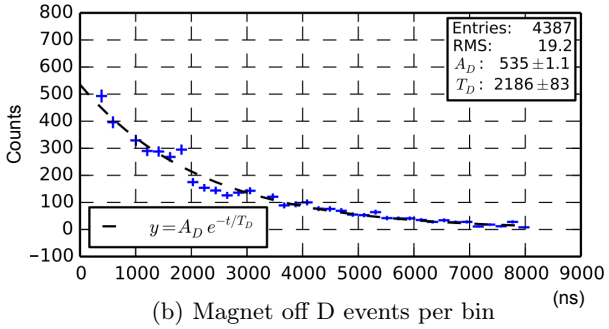

(b) Magnet off D events per bin

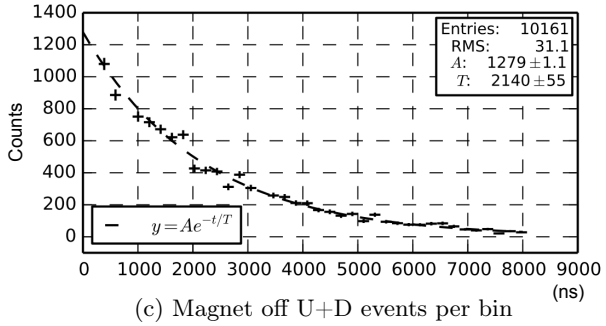

(c) Magnet off U+D events per bin

Figure 7: **Magnet off data with background subtraction**

The third major source of background detections is due to false events, which are independent of decay time. False events occur when one muon (μ^+ or μ^-) registers an M event, and another independent muon or decay process stops one of the TDCs and thereby creates a recorded event. A typical situation is where detector 4 fails to detect a penetrating muon and causes a false M is registered, while another oblique muon avoids detector 1, lands on the target, and decays in time to create a false measurement. Many other similar occurrences involving detection failure and obliquely going muons and positrons contribute to this type of background. As the starting and stopping of the TDCs in these cases are mutually independent, the time intervals measured is approximately evenly distributed, and thus constitute a flat background. However, it is observed that with the subtraction of target out events shown in Figure 6, the flat background is not significant. In other words, there is a good fit for the data that decays with $C = 0$.

The data in Figure 7 show the results for magnet off data with appropriate background subtraction for up, down, and combined events respectively.

The decay lifetime of the combined events is seen to be $T = 2140 \pm 55$ ns.

3.3 Observation of Oscillations

The magnet on data for up, down, and combined events with appropriate background subtractions are shown in Figures 9 and 10.

Before fitting the U minus D events data with the magnet on condition with a sinusoidal equation, the actual start time needs to be calibrated. In the circuit, the start signal of the TDCs is additionally delayed in comparison to the stop signals, in order to prevent the residual current in PMT due to stopped muon to register U and D events. This offset in time is estimated to be 80 ± 10 ns.

After correcting the time origin, the measured decay time of up and down events under all three experiment conditions are sorted into bins of 200 ns wide. The uncertainty of the number of events in each bin is estimated as the square root of the event number in that bin. The time uncertainty is taken as half of the bin width, and the time uncertainty in TDC measurements (20 ns) is negligible in comparison. Notice the bin centered at 700 ns is excluded from all figures except Figure 6, because the TDC used for up event creates a false peak of decay events centered at 670 ns. As shown in Figures 7, 9, and 10, the measured decay time fit well to an exponential function whose characteristic time agrees well with muon mean life time.

The measured event number of each bin is scaled by $e^{t/T}$, where t is the middle time of the bin, and T is the measured mean lifetime found from the combined events magnet off data (see Figure 7c). The difference between the scaled up and down events is then calculated for each bin and a sinusoidal function of the form

$$N_{U-D}(t) = B\,\cos(\omega t) + D \tag{9}$$

is fitted to the data. The constant offset D is introduced to account for the possible difference between the detection efficiency of U and D events. This difference can result from, for example, different detector areas and different PMT high voltages. The plot is shown in Figure 8.

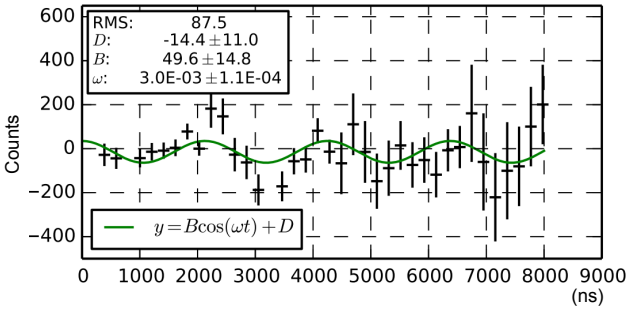

Figure 8: **Scaled U-D data with magnet on**

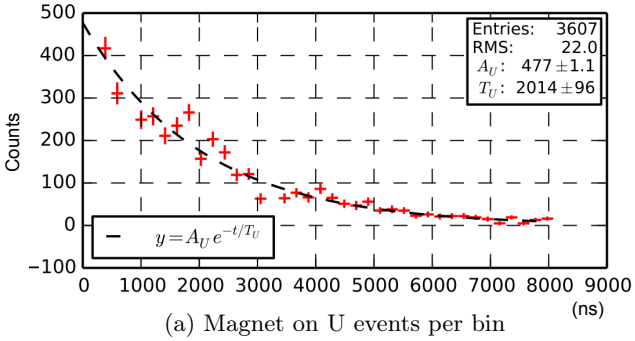

(a) Magnet on U events per bin

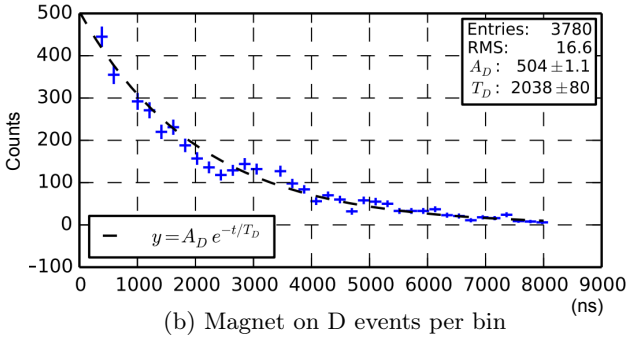

(b) Magnet on D events per bin

Figure 9: **Magnet on data after background subtraction for U and D events separately**

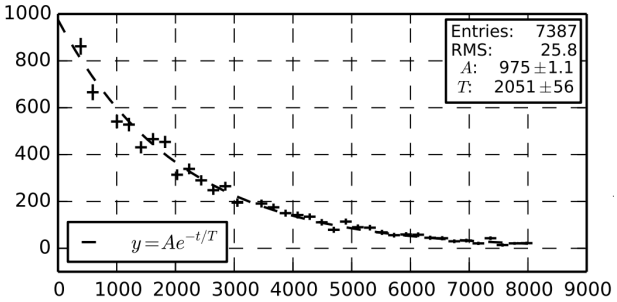

Figure 10: **Magnet on data after background subtraction for U+D**

The χ^2 of the fit in Figure 8 is 29.9 ± 3.41, with a p-value of 0.572 ± 0.169. With this p-value, there is enough statistical evidence to conclude that U minus D events are described by the parameters in Figure 8, which describe an oscillation. Therefore, the experiment observes a non-zero $\langle \hat{\sigma} \cdot \hat{p} \rangle$, which is evidence for the violation of parity in anti-muon weak decay. As an additional step, the decay asymmetry is calculated by the ratio B/A from the magnet on data in Figures 8, 9 and 10. The result is $\alpha = 0.046 \pm 0.014$.

3.4 Error Considerations

One major source of uncertainty in this experiment comes from the statistical fluctuation of the random decay process. The uncertainty in the measured number of events in each bin of decay time is estimated to be the square root of the measured value. The TDC measures time in units of 20 ns, which is thus also estimated to be the uncertainty in each bin's time. These two uncertainties constitute the error bars in the measurements displayed in all previous plots.

The experiment setup can be improved to reduce errors in measurements. For example, increasing the area of detectors and decreasing the separation can significantly reduce false events related to obliquely going muons and positrons.

Three different hardware malfunctions contribute to experiment errors as well. Firstly, the TDC for U events occasionally recorded several muons with very large decay times ($>$ 20 μs), while the TDC is programmed not to record anything if it is not stopped within 20 μs after an M event. These events also occurred very closely within each other. This error is treated by discarding measurements within 10 minutes around each anomaly. The second malfunction was tested to be exclusively related to the TDC for U events as well. An equipment error created a very high and narrow peak in the measured event distribution around $t \approx 700$ ns, which can be seen in the

target out data (Figure 6). This error is treated by ignoring measurements in the 600 ns to 800 ns bin. The last detected hardware error is that the data acquisition computer sometimes records 25% of the decay time to be 0, with no preference to U or D events. This problem is solved by restarting the whole system, but the real cause remains unidentified.

Finally, in order to establish a more convincing correlation between the oscillation of decay events and the precession of the spin vector, the angular frequency ω in Equation 9 should be calculated from the applied magnetic field, instead of being set as a free fitting parameter. For even more convincing results, the applied magnetic field should be varied to observe the dependence of the measured oscillation frequency ω' of decay events on the Larmor frequency ω in Equation 2.

4 Conclusion

This experiment aims to observe parity violation in cosmic anti-muon weak decay. The parity violation is observed by measuring a non-zero mean product of a polar vector and an axial vector. A uniform horizontal magnetic field was applied to polarized cosmic anti-muons stopped in a copper target, which consequently caused the axial spin vector $\hat{\sigma}$ of anti-muons to precess around the magnetic field line. The vertical component of momentum of the positron, produced by anti-muon weak decay, is measured to oscillate with measured decay time at the same frequency as the Larmor precession. As a result, the experiment establishes a non-trivial correlation between $\hat{\sigma}$ and $\hat{p}_z$ with a confidence of 43%, which constitutes an observation of parity violation. Furthermore, we determine the muon mean lifetime to be $T = 2140 \pm 55$ ns and a decay asymmetry of $\alpha = 0.046 \pm 0.014$.

References

[Ali59] A.I. Alikhanyan. Moscow conf. 1. Number 317, 1959.

[DLU62] B.A. Dolgoshein, B. Luchkov, and V. Ushakov. *Phys. JETP*, 15, 1962.

[Gri08] David Griffiths. *Introduction to Elementary Particles*. WILEY-VCH, second, revised edition, 2008.

[OS17] Rene A. Ong and William E. Slater. *Laboratory Manual For Physics 180F*. 2017.

[P+17] C. Patrigani et al. *The Review of Particle Physics*. 2017.

[Sul71] J.D. Sullivan. *Geometrical Factor and Directional Response of Single and Multi-Element Particle Telescopes*. 1971.

Appendix

	Volts
HV 1	1510
HV 2	1450
HV 3	1415
HV 4	1425
HV 5	1575

Table 3: **Final HV values for counters**

Date	Duration/ hrs	Condition
01/28/2018	70	Magnet Off
01/31/2018	24	Magnet Off
02/01/2018	23	Magnet On
02/02/2018	2	Magnet On
02/02/2018	20	Magnet On
02/03/2018	47	Magnet On
02/06/2018	21	Magnet On
02/07/2018	134	Magnet On
02/13/2018	54	Magnet Off
02/15/2018	123	Magnet On
02/27/2018	102	Target Out
03/03/2018	70	Target Out
03/06/2018	120	Magnet Off

Table 4: **Data log for data collection**

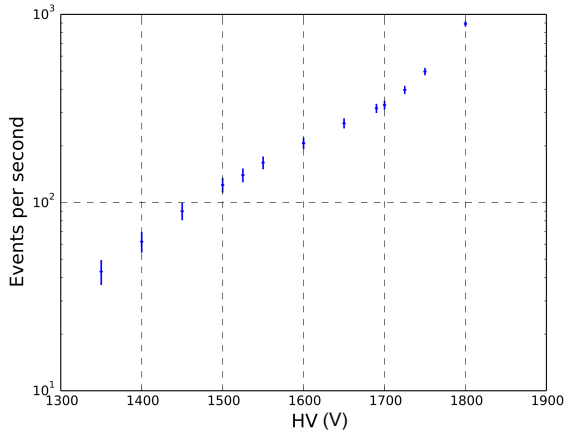

(1) PMT 2

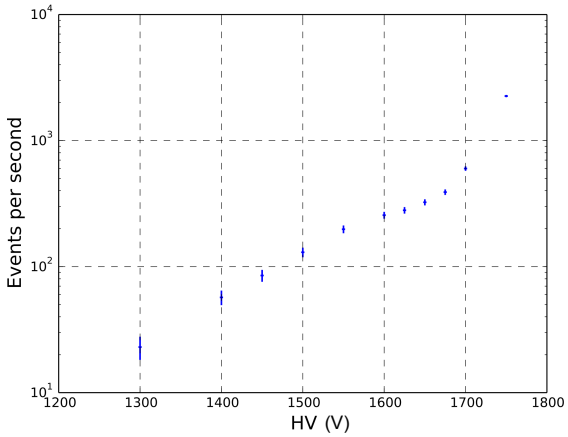

(2) PMT 3

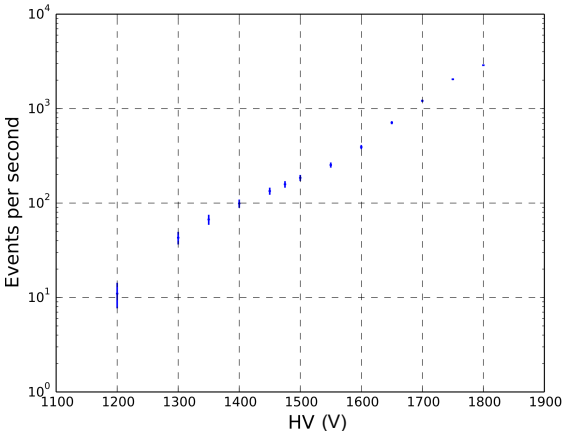

(3) PMT 4

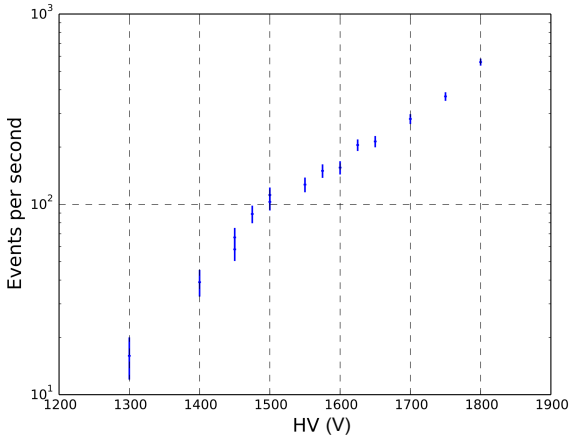

(4) PMT 5

Figure A: **Single Rates for PMT 2 through 5**

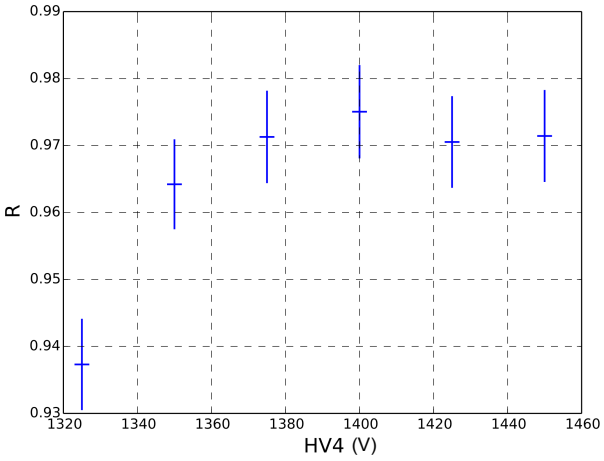

Figure B: **Coincidence method plot of C3, 4, 5 using HV3=1365V and HV5=1525V**